BIOCHEMISTRY
including biophysical chemistry & molecular biology

Article

pubs.acs.org/biochemistry

Structure, Function, and Chemical Synthesis of *Vaejovis mexicanus* Peptide 24: A Novel Potent Blocker of Kv1.3 Potassium Channels of Human T Lymphocytes

Georgina B. Gurrola,[†] Rogelio A. Hernández-López,[‡,@] Ricardo C. Rodríguez de la Vega,[§] Zoltan Varga,[∥] Cesar V. F. Batista,[†,⊥] Saida P. Salas-Castillo,[†] Gyorgy Panyi,[∥] Federico del Río-Portilla,[‡] and Lourival D. Possani*[,†]

[†]Departamento de Medicina Molecular y Bioprocesos, Instituto de Biotecnología, Universidad Nacional Autónoma de México, Av. Universidad, 2001 Cuernavaca, Mor. 62210, Mexico

[‡]Instituto de Química, Universidad Nacional Autónoma de México, Circuito Exterior, Ciudad Universitaria Mexico, DF 04510, Mexico

[§]Ecologie, Systématique et Evolution, Université Paris-Sud, F-91405 Orsay cedex, France; UMR 8079, CNRS, F-91405, Orsay cedex, France

[∥]Department of Biophysics and Cell Biology, Medical and Health Sciences Center, University of Debrecen, Debrecen, 4012 Hungary

[⊥]Laboratorio Universitario de Proteómica, Instituto de Biotecnología, Universidad Nacional Autónoma de México, Cuernavaca, Mor. 62210, Mexico

Supporting Information

ABSTRACT: Animal venoms are rich sources of ligands for studying ion channels and other pharmacological targets. Proteomic analyses of the soluble venom from the Mexican scorpion *Vaejovis mexicanus smithi* showed that it contains more than 200 different components. Among them, a 36-residue peptide with a molecular mass of 3864 Da (named Vm24) was shown to be a potent blocker of Kv1.3 of human lymphocytes (K_d ~ 3 pM). The three-dimensional solution structure of Vm24 was determined by nuclear magnetic resonance, showing the peptide folds into a distorted cystine-stabilized α/β motif consisting of a single-turn α-helix and a three-stranded antiparallel β-sheet, stabilized by four disulfide bridges. The disulfide pairs are formed between Cys6 and Cys26, Cys12 and Cys31, Cys16 and Cys33, and Cys21 and Cys36. Sequence analyses identified Vm24 as the first example of a new subfamily of α-type K^+ channel blockers (systematic number α-KTx 23.1). Comparison with other Kv1.3 blockers isolated from scorpions suggests a number of structural features that could explain the remarkable affinity and specificity of Vm24 toward Kv1.3 channels of lymphocytes.

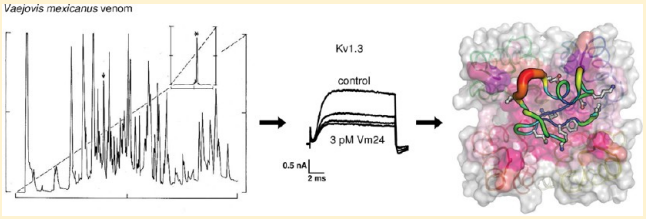

Blockers of ion channels have significant therapeutic potential in the management of diseases affecting excitable tissues. It is well established that ion channels are also required for the proper physiological function of classically nonexcitable cells such as lymphocytes.[1] In this sense, a key step in the generation of an efficient immune response and protection of the organism against various infectious agents is the antigen-induced activation and proliferation of T cells that can be inhibited by the blockers of plasma membrane K^+ channels. Autoimmune diseases are characterized by the generation of autoreactive T cell clones that react to self-antigens, thereby leading to the destruction of specific tissues, such as myelinated neurons in multiple sclerosis or insulin-producing pancreatic β cells in type I diabetes mellitus.[2] The proliferation of the autoreactive T cells mediating tissue damage [effector memory T cells (T_{EM})] can be specifically and persistently inhibited by blockers of Kv1.3 potassium channels. This underlines the therapeutic potential of high-affinity and high-specificity Kv1.3 inhibitors.[3]

Several naturally occurring peptides, especially from scorpion venom and sea anemone, have been reported to be effective blockers of the Kv1.3 channels.[3] Most peptides purified from scorpion venom sources and reported to affect Kv channels have been isolated from species of the family Buthidae, with relatively few examples from other scorpion families and none from Vaejovidae. Four distinct types of K^+ channel blocking peptides from scorpion venoms have been described: α-, β-, γ-, and κ-KTx.[4−6] The α-KTx peptides contain 23−42 residues adopting a cystine-stabilized α/β motif with three or four disulfide bridges.[4] These are further classified into 22 subfamilies according to sequence relatedness.[6,7] Although

Received: January 13, 2012
Revised: April 27, 2012
Published: April 27, 2012

 © 2012 American Chemical Society

several α-KTx peptides are potent blockers of Kv1.3 channels, most of them also block other K^+ channels with similar affinities,[3] therefore lowering their therapeutic potential.[8]

Toxin variants with improved selectivity for Kv1.3 have been obtained by introducing substitutions for natural amino acids into key positions of OSK-1/α-KTx 3.7 (e.g., [K16,D20]-OSK1[9]) and BmKTx/α-KTx 3.6 ([R11,T28,H33]-BmKTx, also named ADWX-1[10]). The specificity for Kv1.3 channels of the structurally unrelated sea anemone peptide named ShK[11,12] has been successfully increased by introducing a non-natural amino acid (ShK-Dap22[13]) or various N-terminal modifications (e.g., ShK-192[14]). More recently, an engineered peptide, selected from a phage display library based on 31 α-KTx peptides, was shown to possess an improved selectivity for Kv1.3 channels.[15]

In this work, we report the first K^+ channel blocking peptide isolated from the venom of the Mexican scorpion *Vaejovis mexicanus smithi* (abbreviated hereafter *Vm smithi*). The soluble venom of *Vm smithi* was separated by high-performance liquid chromatography (HPLC) and individually collected in ∼80 subfractions. Proteomic analysis of these subfractions showed that it contains more than 200 components with distinct molecular masses. Vm24, one of the purified peptides, was shown to be a potent and selective blocker of the Kv1.3 channels of human peripheral blood T lymphocytes, also inhibiting their proliferation (Z. Varga, G. Gurrola-Briones, F. Papp, R.C. Rodríguez de la Vega, G. Pedraza-Alva, R.B. Tajhya, R. Gáspár, L. Cardenas, Y. Rosenstein, C. Beeton, L.D. Possani, G. Panyi, manuscript submitted to Molecular Pharmacology for publication). The full covalent structure of Vm24 was determined, and the chemical synthesis and correct folding of this peptide were obtained and characterized. The three-dimensional structure was also determined by solution NMR spectroscopy. Both the primary structure and the tertiary structure of this peptide are considerably different from those of all other known α-KTx peptides; thus, Vm24 defines a new subfamily of α-KTx. A comparative docking of Vm24 and Kv1.3 highlighted a number of structural features that could explain its remarkable blocking potency and selectivity for Kv1.3 channels.

MATERIALS AND METHODS

Isolation and Characterization of Vm24. *Chromatographic Separation and Proteomic Analysis of Components.* The soluble venom of *Vm smithi* was separated by HPLC using a C18 reverse phase column (from Vydac, Hesperia, CA). A linear gradient from solvent A (0.12% TFA in water) to 60% solvent B (0.10% TFA in acetonitrile) was applied to the column and run for 60 min. The effluent was collected separately and immediately freeze-dried. The molecular mass of each subfraction was evaluated by mass spectrometry analysis using a Finnigan LCQ^{Duo} apparatus, as described previously.[16] Fractions containing molecular masses in the range expected for K^+ channel blockers (4000 Da) were selected for electrophysiological assays. Among these fractions was one eluting at 24 min. This fraction was rechromatographed under similar conditions (see the details in the figure legends), producing a homogeneous peptide dubbed Vm24.

Lethality Tests Conducted in Vivo. The mouse model was used to assess the existence of possible toxic effects of Vm24. Mice treated intraperitoneally with various amounts of soluble venom from *Vm smithi* [from 50 to 200 μg of protein per mouse (20 g body weight)] showed no symptoms of intoxication. However, to be sure that the purified peptide caused no harm to the same animal model, highly pure native Vm24 and synthetic Vm24 at doses of 50−200 μg/20 g mouse were also tested.

Determination of Amino Acid Sequences. A sample of native Vm24 (approximately 1 nmol of protein) was directly loaded into a Beckman (Palo Alto, CA) LF3000 Protein Sequencer with chemicals and procedures provided by the company. The N-terminal amino acid sequence was unequivocally assigned. Analysis conducted with various aliquots of the reduced and alkylated peptide was used for confirmation of the cysteine residues and for digestion with endopeptidases. The digestion of reduced Vm24 with ArgC-endopeptidase (Roche Diagnostics, Basel, Switzerland) and trypsin (Boehring, Mannheim, Germany), using conditions described previously by our group,[16] permitted separation by HPLC of several subpeptides that under sequence analysis by Edman degradation and mass spectrometry fragmentation allowed us to obtain a unique primary structure, as indicated in the figure legends.

Sequence Analysis and Phylogenetic Reconstruction. Multiple-sequence alignment of Vm24 with several scorpion venom-derived Kv1.3 blockers was performed with CLUSTAL_X.[17] Phylogenetic tree reconstruction was performed using Bayesian inference, essentially as described previously[18] with MrBayes version 3.1.2[19,20] using a multiple-sequence alignment of 101 α-KTx sequences. The procedure estimates the posterior probability of a given tree topology by a Markov chain Monte Carlo (MCMC)-based sampling procedure over $n - 1$ stochastically generated trees. One Markov chain remains heuristically searching within the tree topology with the best posterior probability at a given step of the sampling procedure, evaluated under a specified amino acid substitution model (the overall process is called Metropolis coupling MCMC or MC^3). For this analysis, four chains with 250000 trees each were generated under the JTT amino acid substitution model and sampled every 250th iteration. Coalescence was obtained at approximately 175000 iterations, and the 250 remaining trees with best posterior probabilities were merged to calculate a 50% majority rule consensus tree.

Determination of Disulfide Pairing. The disulfide bridges of Vm24 were determined by digesting a sample containing 25 μg of native Vm24 with an equal amount (0.5 μg each) of chymotrypsin (Boehring) and trypsin in 150 mM Tris-HCl (pH 6.8) for 12 h at 37 °C. The generated peptides were separated by HPLC using the same conditions that were described for the venom separation (see above). Individual peptides were analyzed by mass spectrometry fragmentation (MS/MS) from which the amino acid sequence was obtained. Because the primary structure was known, the assignment of the disulfide bridges could be inferred.

Chemical Synthesis and Folding of Vm24. A linear analogue of Vm24 was synthesized by a solid phase methodology on rink amide MBHA resin (Calbiochem-Novabiochem Corp., San Diego, CA). Fmoc-amino acids (Calbiochem-Novabiochem Corp.) were used with the following side chain protection: Arg(Pbf), Asn(Trt), Cys(Trt), Gln(Trt), Glu(OtBu), Lys(Boc), Ser(tBu), and Tyr(tBu). The Fmoc group was removed by treatment with 20% piperidine in dimethylformamide (DMF) for 20 min followed by a wash with DMF. Fmoc- amino acids (0.5 mmol) were coupled as active esters, which was preformed in DMF with HBTU [2-(1*H*-benzotriazol-1-yl)-1,1,3,3-tetramethyluronium hexafluorophosphate] and DIEA (diisopropylethylamine) (0.45 and 0.75 mmol, respectively; activation for 2 min) as activating agents. Coupling times were 30 min. Unreacted or deblocked free

amines were monitored through the ninhydrin test,[21] in every cycle of the peptide synthesis. During the entire synthesis, before the next amino acid was coupled, the undesirable residual free amines were blocked by acetylation. All the operations were performed manually in a 50 mL glass reaction vessel with a Teflon-lined screw cap. The peptide resin was agitated by gentle inversion during the Nα-deprotection and coupling steps.

Following final removal of the Fmoc group, the peptide resin (1.7 g) was cleaved from the resin and simultaneously deprotected using reagent K[22] for 2 h at room temperature. Following cleavage, the crude peptide was precipitated and washed with ice-cold *tert*-butyl ether and then dissolved in 20% aqueous acetic acid. The product was lyophilized and kept desiccated at −20 °C until it was used.

The cyclization reaction to make the corresponding disulfide bridges of the molecule was conducted in 0.1 M NaCl, 5 mM reduced glutathione, 0.5 mM oxidized glutathione, 20 mM Na_2HPO_4 (pH 7.8), and 30 μM unfolded synthetic Vm24. The crude cyclized product was purified in two steps by HPLC. The first used a C18 preparative column (238TP1022 Vydac), with a linear gradient of solution A (0.12% TFA in water) to solution B (0.1% TFA in acetonitrile) run up to 60% B over 60 min. The principal component from this chromatographic step was separated using a C18 analytical column (218TP54 Vydac) run with linear gradient from solvent A to 40% solvent B in 60 min.

Determination of the NMR Structure. *NMR Methods.* A sample of synthetic purified Vm24 containing 5 mg of peptide was dissolved in 0.3 or 0.65 mL of an H_2O/D_2O mixture (9.5:0.5, v/v) to a final concentration of 1.9 or 0.9 mM, respectively. After the experiments in H_2O, the peptide was lyophilized and redissolved in D_2O for additional experiments.

^{1}H NMR Spectroscopy. The experiments were performed in a Varian Unity Plus 500 or an Inova 600 spectrometer (both from Varian Inc., Palo Alto, CA) using a 5 or 3 mm HCN indirect detection probe. Samples were prepared in a 95:5 H_2O/D_2O mixture or 100% D_2O. The pH of the sample was 6.5. Data were collected at 300 K. Mixing times were 35 and 75 ms for TOCSY and 80, 100, 200, and 400 ms for NOESY in both solvents. Data were processed with NMRPIPE[23] using 2K × 2K data points in all NMR experiments. Spectra were analyzed using XEASY.[24]

Experimental Constraints and Structure Calculations. The H1 resonances were assigned with standard homonuclear NMR techniques,[25] using DQ-COSY,[26] TOCSY,[27] and NOESY[28] experiments. Most of the distance constrains were obtained from NOESY spectra in H_2O; additional constraints were from NOESY D_2O spectra. NOE intensities were evaluated from the volume of the cross-peaks and calibrated internally using CALIBA[29] to generate a set of upper limit distances. Most NOE data were obtained from resolved signals and by automatic assignments using CYANA 2[30] with a simulated annealing algorithm. NOEs are plotted in the corresponding figure below.

A total of 200 structures were generated with CYANA using 315 dihedral angle constraints and 477 unambiguously assigned distance constraints which include 314 short-range, 104 medium-range, and 59 long-range constraints (Table S2 of the Supporting Information). The 20 CYANA structures with the lowest CYANA target function values were used for further molecular dynamics (MD) refinement in explicit solvent using AMBER 9.[31] A total of 315 dihedral angle constraints and 455 distance constraints were used for the AMBER calculation. The distance constraints include 275 short-range, 45 medium-range, and 135 long-range constraints. These constraints were used for all simulations except for the first 300 ps of each explicit water simulation.

Molecular Dynamics Simulations. All the molecular dynamics simulations and the energy minimizations were conducted using the topology and force field parameters of the AMBER-99SB force field.[32] We followed one of the refinement protocols proposed by Xia and co-workers[33] with some modifications.

For the MD refinement in vacuum, the 20 CYANA structures were first energy minimized. Then two cycles of 30 ps MD simulated annealing from 1000 to 0 K considering the NMR constraints were performed. A final 2000-step energy minimization with NMR constraints was performed. A cutoff of 15.0 Å was used for calculation of long-range interactions. For the explicit water refinement, the 20 previously minimized structures were used as initial structures. A solvent box and chloride atoms as counterions were added to solvate and neutralize the system. In explicit water calculations, a cutoff of 10.0 Å was used for computation of long-range interactions, where three-dimensional periodic boundary conditions were applied. The initial structures were subjected to three cycles of 40 ps of MD with a constant volume, with gradual heating from 0 to 50 K, from 50 to 100 K, and from 100 to 300 K, with 5 kcal mol^{-1} Å^{-2} harmonic constraints on the protein. These were followed by two cycles of 40 ps constant-pressure MD (*NPT* ensemble) with pressure relaxation times of 0.2 and 1.0 ps, with 5 kcal mol^{-1} Å^{-2} harmonic constraints on the protein. The temperature and pressure were kept stable at 300 K and 1 bar, respectively. Then, another 40 ps constant-volume MD with 5 kcal mol^{-1} Å^{-2} harmonic constraints on the protein was applied. This was followed by a 60 ps constant-volume MD with a decreased force constant on the protein of 0.5 kcal mol^{-1} Å^{-2}.

Finally, a 100 ps MD simulation (*NVT* ensemble) with a time step of 1 fs without harmonic constraints on the protein coordinates was conducted at 300 K. The total simulation time for each structure is thus 400 ps. After the final MD cycle, a 2000-step energy minimization in explicit solvent using the conjugated gradient method under the NMR constraints was performed. Superposition of the 20 refined structures shows an rmsd of 1.403 Å for all heavy atoms (Table S3 of the Supporting Information). More than 95% of the residues are located within most favored and additional allowed regions as shown by Ramachandran analysis (Figure S1 of the Supporting Information).

NMR Solution Structure of Vm24. The Vm24 secondary structure was first deduced from NOE characteristic patterns between backbone protons (H^α and H^N) and finally established with results of the tertiary structure calculations. The two outer strands of the β-sheet, S1 (residues 4 and 5) and S2 (residues 23−26), are connected by a not well-defined α-helix (residues 13−16) because of the absence of enough NMR constraints. Two consecutive prolines could explain this result (residues 13 and 14). Strand S3 (residues 30−34) is in the center. A coil is formed between residues 6 and 12 where proline 13 is very likely impeding the formation of a well-defined secondary structure. All three prolines are *trans* isomers. The tertiary structure is an α/β-scaffold with a very short helix. Four disulfide bridges restrict the general folding and link the β-sheet with the α-helix and the coils. Accordingly with the structure

dx.doi.org/10.1021/bi300060n | *Biochemistry* 2012, 51, 4049−4061

superposition, regions between residues 7−9 and 17−20 are not well-defined because of the absence of NOEs. Only the disulfide bridge between Cys21 and Cys36 is localized to connecting coils, whereas the others connect secondary structure elements.

Electrophysiology. *T Lymphocytes for Patch-Clamp Recording.* Heparinized human peripheral venous blood was obtained from healthy volunteers. Mononuclear cells were separated by Ficoll-Hypaque density gradient centrifugation. Collected cells were washed twice with Ca^{2+} and Mg^{2+} free Hank's solution containing 25 mM HEPES buffer (pH 7.4). Cells were cultured in a 5% CO_2 incubator at 37 °C in 24-well culture plates in RPMI-1640 supplemented with 10% fetal calf serum, 100 μg/mL penicillin, 100 μg/mL streptomycin, and 2 mM L-glutamine at a density of 0.5×10^6 cells/mL for 3−4 days. The culture medium also contained 6 or 8 μg/mL phytohemagglutinin A to improve K^+ channel expression.[34] T lymphocytes were selected for recording human Kv1.3 currents by incubation with mouse anti-human CD2 followed by selective adhesion to Petri dishes coated with goat anti-mouse IgG antibodies, as described by Matteson and Deutsch.[35] Dishes were washed gently five times with 1 mL of normal extracellular bath medium (see below) for the patch-clamp experiments.

Recording Conditions and Solutions. Whole-cell currents[36] were measured in voltage-clamped cells using Axopatch 200A and Multiclamp 700B amplifiers connected to a personal computer using Axon Digidata 1200 and 1322A data acquisition hardware, respectively (Molecular Devices Inc., Sunnyvale, CA). Series resistance compensation up to 70% was used to minimize voltage errors and achieve good voltage-clamp conditions. Pipettes were pulled from GC 150 F-15 borosilicate glass capillaries in five stages and fire-polished, resulting in electrodes having resistances of 3−5 MΩ in the bath. The bath solution consisted of 145 mM NaCl, 5 mM KCl, 1 mM $MgCl_2$, 2.5 mM $CaCl_2$, 5.5 mM glucose, and 10 mM HEPES (pH 7.35), supplemented with 0.1 mg/mL bovine serum albumin. The measured osmolarity of the external solutions was between 302 and 308 mOsm/L. The internal solution consisted of 140 mM KF, 2 mM $MgCl_2$, 1 mM $CaCl_2$, 10 mM HEPES, and 11 mM EGTA (pH 7.22). The measured osmolarity of the internal solutions was approximately 295 mOsm/L. Bath perfusion around the measured cell with different test solutions was achieved using a gravity-flow perfusion system. Excess fluid was removed continuously.

Data Analysis. For data acquisition and analysis, pClamp8/10 (Molecular Devices Inc.) was used. Generally, currents were low-pass-filtered using the built-in analog four-pole Bessel filters of the amplifiers and sampled (2−50 kHz) at least twice the filter cutoff frequency. Before analysis, whole-cell current traces were corrected for ohmic leakage and digitally filtered (three-point boxcar smoothing). Data points for the dose−response curve were fit with a two-parameter Hill equation: $RCF = K_d^n/(K_d^n + [Tx]^n)$, where RCF is the remaining current fraction ($RCF = I/I_0$, where I and I_0 are the current amplitudes in the presence and absence of the toxin at a given concentration, respectively), K_d is the dissociation constant, n is the Hill coefficient, and [Tx] is the toxin concentration. Each data point on the dose−response curve represents the mean of three to seven independent experiments, and error bars represent the standard error of the mean (SEM).

Structural Comparisons and Docking. Structural alignments were performed with TopMatch.[37] The three-dimensional structures of Vm24 [Protein Data Bank (PDB) entry 2k9o], ADWX-1 (PDB entry 2k4u[38]), Mokatoxin (PDB entry 2kir[15]), and Maurotoxin (PDB entry 1txm[39]) were docked onto the models of Kv1.3 and KCa3.1 channels with RosettaDock.[40] Monomeric pore-forming segments of the channels were homology modeled on the basis of the coordinates of the rKv1.2 channel (PDB entry 3lut[41]) with the Swiss Model suite.[42] Tetrameric channels were built with the symmetry parameters of the template with the PDBe PISA web server[43] and further refined with Modeller 9v2[44] as described previously.[45] The RosettaDock server currently runs the Rosetta 2.1 suite[46] to search the rigid body and side chain conformational space of a given protein complex to identify low-energy conformations of the protein−protein interaction. The initial "approximate binding orientation" required by the program was constructed for each interaction pair by superimposing the structures (toxins) and models (channels) on the complex between charybdotoxin and a mutant KcsA channel,[47] using PyMOL.[48] Several PyMOL scripts were based on R. L. Campbell's repository (http://pldserver1.biochem.queensu.ca/~rlc/work/pymol/). Unless otherwise stated, the final structural analyses were conducted with the 20 best scoring models in the pore-blocking mode.

RESULTS

Proteomics of *Vm smithi* Venom. Under the chromatographic conditions described in the previous section, at least 80 distinct fractions can be identified from the soluble venom of *Vm smithi* (Figure 1A). Each subfraction was separately collected and used for the physiological assay and proteomic analysis, as described below. The results of the proteomic analysis of the soluble venom of *Vm smithi* are listed in Table S1 of the Supporting Information and Figure 1B. This analysis revealed that at least 200 different components are present in this venom. The various components registered were analyzed and grouped according to molecular mass in increments of 1500 Da. More than 90% of the components identified have molecular masses of <6001 Da. Three groups had at least 60 different components. They fall within the ranges of 117−1500, 1501−3000, and 3001−4500 Da. These results were important for choosing the appropriate peptides for functional analysis (peptides in the range of 3001−4500 Da). The rationale follows the known molecular mass of K^+ channel blocking toxins from scorpion venoms.[16,49,50]

Purification and Covalent Structure of Vm24. Among the fractions chosen for further analysis, the one eluting at 24 min was rechromatographed (see the inset of Figure 1A), producing a homogeneous peptide, here called Vm24. Direct Edman degradation and mass spectrometry analysis of Vm24 fragments generated by enzymatic hydrolysis revealed that this peptide has 36 amino acid residues (Figure 2A). Initial sequencing of Vm24 gave an unequivocal amino acid sequence for the first 23 amino acid residues. Two peptides obtained by Arg-C1 cleavage allow the identification of the sequences ranging from residue A18 to R29 and from residue K30 to C36. The overlap was obtained with two additional peptides, one from a tryptic digestion that allowed the identification of residues from C26 to K32, and a confirmatory peptide obtained from Lys-C digestion that corresponded to residues from C33 to C36. The peptide is amidated in its C-terminal amino acid, as found by mass spectrometry analysis (Figure 2B). A comparison of the molecular masses reduced and oxidized forms of Vm24 shows an exactly 8 Da difference; the

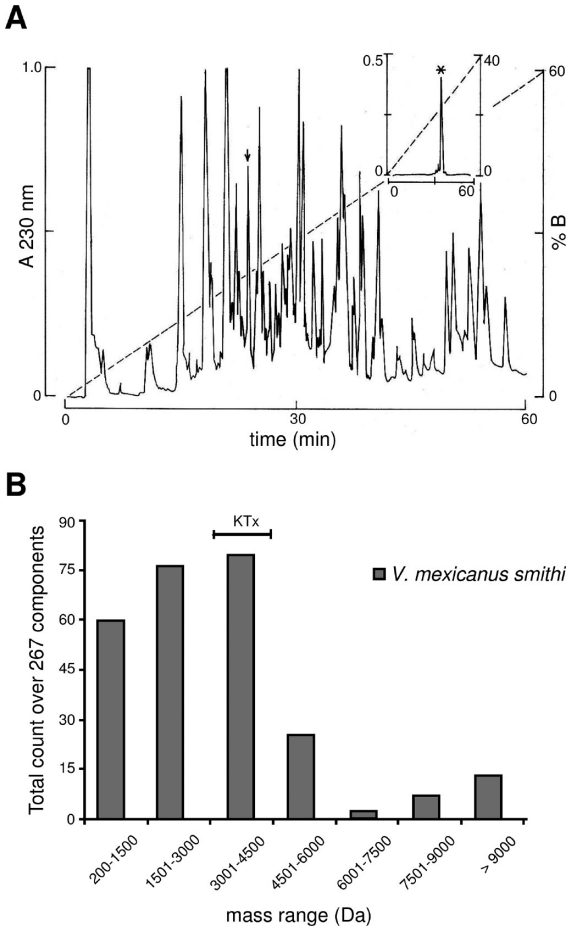

Figure 1. HPLC separation of the venom and proteomic analysis. (A) One milligram of soluble venom from *Vm smithi* was separated by HPLC in a C18 reverse phase column using a linear gradient from solvent A (water in 0.12% TFA) to 60% solvent B (0.10% TFA in acetonitrile). The component labeled with an arrow was further separated using a gradient from 0 to 40% solvent B (in the inset, component labeled with an asterisk). (B) Distribution histogram of identified masses. The mass range for K^+ specific toxins is indicated; more than 75 *Vm smithi* venom components fall within this range.

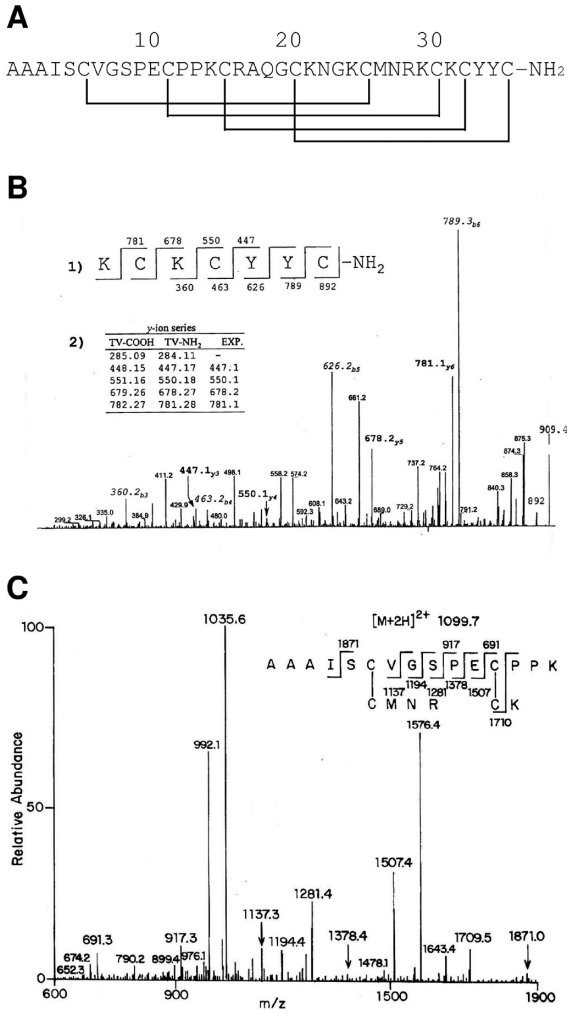

Figure 2. Sequence analysis of Vm24. (A) Full sequence of Vm24, including cysteine pairing. The full covalent sequence was determined by Edman degradation and mass spectrometry using the native peptide, reduced and alkylated samples, and fragments generated by enzymatic hydrolysis as described in Materials and Methods. The disulfide pairing as indicated was obtained by mass spectrometry analysis of peptides produced from the native peptide digested with hydrolytic enzymes (see details in Material and Methods and below). (B) Vm24 possesses an amidated C-terminus. Collisional-induced dissociation (CID) of the C-terminal $[M + H]^+$ ion at 909.4 Da (monoisotopic molecular mass) shows a value 1.0 unit less than the expected theoretical value of $[M + H]^+$ 910.5 Da The y ion series (italic) corresponding to an amidated C-terminal sequence is shown in the inset labeled 1). Theoretical y ion series values for free carboxy-terminal peptide (TV-COOH), theoretical y ion series values for the amidated C-terminus (TV-NH_2), and experimental y ion series values (EXP.) are compared in the table. (C) Mass spectrometry showing the disulfide Vm24 cysteine half-pairs. It shows the mass spectrum corresponding to the structure of the complex core containing both cysteine half-pairs, C1−C4 and C2−C6 with the $[M + 2H]^{2+}$ ion at 1099.7 Da. The b ion series values from 1137 to 1507 Da unequivocally represent the GSPE tag, confirming the assignment of the last two cysteine half-pairs. These results support the data presented in panel A, where the disulfide pairings are indicated.

experimental molecular mass found for the native peptide was 3864.0 Da and for the completed reduced peptide was 3872.0 Da, confirming that all eight cysteines are involved in disulfide bridge formation. Three main peptide fragments were obtained from simultaneous chymotrypsin and trypsin digestion at pH 6.8 (slightly acidic pH to prevent mixed disulfide rearrangements), showing monoisotopic molecular masses of $[M + H]^+$ 788.0 Da, $[M + H]^+$ 560.4 Da, and $[M + 2H]^{2+}$ 1099.7 Da. The peptide with a mass of $[M + H]^+$ 788.0 Da corresponds exactly to the expected molecular mass of the cysteine pairs (Cys21−Cys36) of the heterodimer amino acid sequence AQGCK-YC. The second disulfide bridge determined was that from Cys16 to Cys33 that has equal theoretical and experimental values of 560.4 Da (CR-CY sequences). Both peptides were further characterized by collision-induced dissociation (CID) experiments showing the expected amino acid sequences. The signal at m/z $[M + 2H]^{2+}$ 1099.7 Da (deconvoluted mass of 2197.4 Da) comes from the heterodimer core containing the last two cysteine half-pairs (Figure 2C). This fragment was directly analyzed. The CID ion series from the signal at m/z $[M + 2H]^{2+}$ 1099.7 Da shows two ion values that satisfy the condition for the complete determination of the last two cysteine pairs. The b ion at 1507.4 Da and the y ion at 691.3 Da that are products of the same amide cleavage bond between the glutamic acid (E11) and cysteine (C12) clearly assign the Cys6−Cys26 and Cys12−Cys31 half-pairs. Furthermore, the in

dx.doi.org/10.1021/bi300060n | *Biochemistry* 2012, 51, 4049−4061

tandem fragmentation values from the b ion at 1710.5 Da to the b ion at 1137.3 Da characterize the internal tag (GSPEC-C) with unequivocal mass values confirming the disulfide bridge arrangement schematically represented in Figure 2A. The NMR data confirmed these disulfide assignments (see below).

Chemical Synthesis. The profile of the chromatogram obtained after chemical synthesis and folding of Vm24 is shown in Figure 3A. The main component was finally purified using a C18 analytical column (218TP54 Vydac) run with linear gradient from solvent A to 40% solvent B in 60 min (inset of Figure 3A). The structure and purity of the synthetic toxin were confirmed by analytical HPLC and amino acid sequence and mass spectrometry determination. The correctness of the amino acid sequence was verified by direct Edman degradation up to residue 30. The elution time from the HPLC column coincided exactly with the time at which the native peptide elutes from the same column under identical conditions. Examples of the elution pattern obtained with native Vm24 (letter A), synthetic Vm24 as described here (letter B), and an equimolar mixture of native and synthetic Vm24 (letter C) are shown in Figure 3B. The molecular mass determined by mass spectrometry was 3864 Da, showing that it corresponds exactly to that of the expected sequence. It is worth noting that the resin used is designed for the production of a C-terminally amidated peptide, exactly like the case for native Vm24. From ~1.7 g of resin containing the synthetically prepared peptide with the expected primary sequence of Vm24, ~300 mg of the correctly folded peptide was obtained, representing a yield of 30% of the theoretical expected value (from the starting resin). The physiological effects of the synthetic Vm24 were shown to be indistinguishable from that of the native peptide (see below).

Determination of the Three-Dimensional Structure by NMR. The structure of Vm24 was determined by solution NMR methods. The regular secondary structure elements identified on the basis of characteristic sets of specific and short interproton distance analyses are presented below the sequence in Figure 4 as the chemical shift index. The pattern of short-range NH^{i}–NH^{i+1} NOEs associated with weak $H^{\alpha i}$–NH^{i+1} connectivities indicates the presence of a small α-helix extending from residue 13 to 16. Furthermore, weak typical medium-range $H^{\alpha/i}$–NH^{i+2} cross-peaks could be observed. The structure consists of a triple-stranded antiparallel β-sheet (residues 4 and 5, 23–26, and 30–34 for S1–S3, respectively) and a noncanonical helix (residues 13–16), conforming to an atypical cysteine-stabilized α/β-scaffold (Figure 5). Residues in positions 7–9 and 17–20 are not well-defined because of a reduced number of NOEs, in comparison with other regions (Figure 5A). The relative orientation of the secondary structure is defined by four disulfide bridges. Two of them (Cys12–Cys31 and Cys16–Cys33) connect the helix with the C-terminal strand (S3) of the β-sheet. The disulfide bridge established with Cys6 and Cys26 connects the end of S1 and the end of S2, whereas Cys21 and Cys36 are localized in coils. Figure 5B shows the electrostatic potential surface calculated using APBS.[51] Electrostatic potential is displayed on a molecular surface with a color scale from −3 to 3 kBT/ec. Visualizations were made using VMD.[52] Cysteines and Ile4 are completely buried, and all other residues are exposed. Interestingly, Tyr35 and Cys36 are in a flexible region, despite the disulfide bridge. The three-dimensional coordinates obtained are deposited as PDB entry 2k9o. See additional

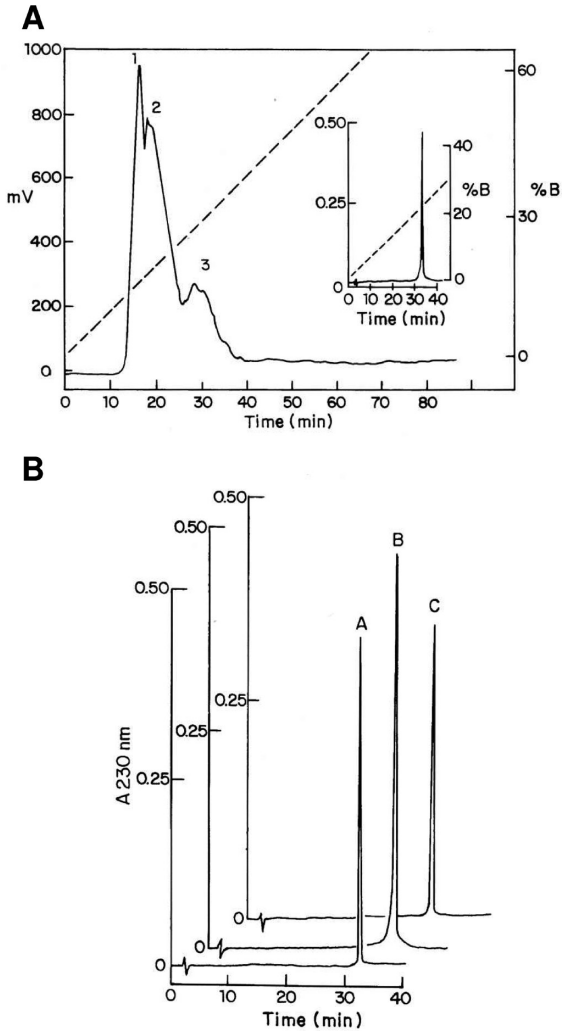

Figure 3. Purification of synthetic Vm24. (A) HPLC separation of chemically synthesized Vm24. An aliquot of Vm24 (50 mg of protein) was separated in a C18 reverse phase preparative column. The number 1 indicates the elution position of synthetic and correctly folded Vm24, whereas numbers 2 and 3 indicate incorrectly folded or truncated sequences. An additional separation of this chromatographic fraction was conducted in the same system, but using an analytical column developed with a linear gradient from solution A to 40% solution B over 60 min. The results are shown in the inset. (B) HPLC comparison of synthetic and natural Vm24 peptides. Application of 10 μg of native Vm24 to an analytical C18 column shows that the pure peptide elutes at 32.67 min (labeled with the letter A). Application of 15 μg of synthetically prepared and folded Vm24 to the same system and under the same conditions showed similar separation (labeled with the letter B). Finally, co-injection of a 1:1 mixture of synthetic and natural Vm24 (total of 8 μg) shows that they co-elute at the same retention time (labeled with the letter C). It is worth mentioning that the *x*-axis of the graph is shifted to the right for letters B and C, so that the three graphs could be observed comparatively, but separately; otherwise, the elution times of the three independent HPLC runs would fall into the same peak and become indistinguishable.

confirmatory data in Figure S1 and Table S2 of the Supporting Information.

Functional Analysis Using Kv1.3 Channels of T Cell Lymphocytes and in Vivo Assays Using Mice as Experimental Animals. These structural characteristics make Vm24 an exceptional scorpion venom peptide; hence, we tested if such unique structural features of Vm24 are

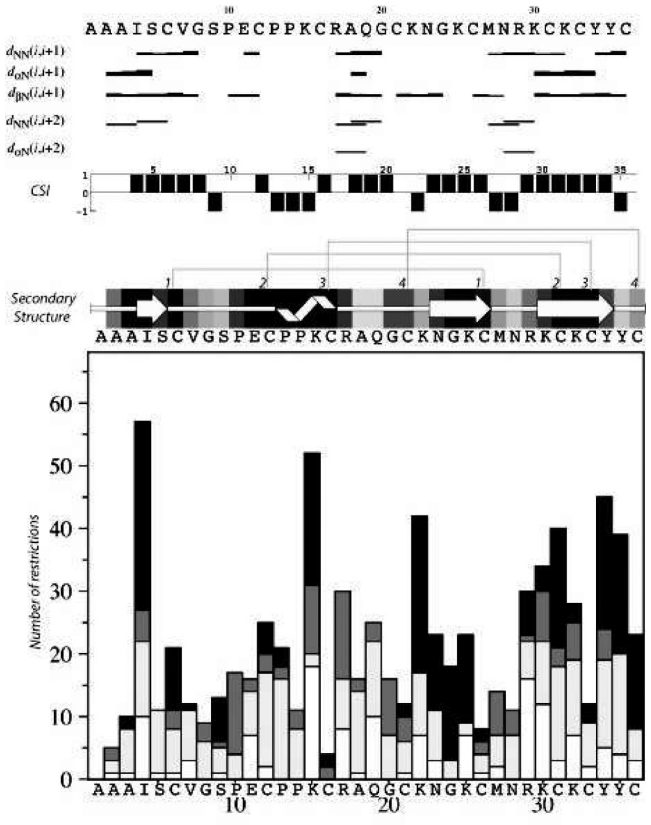

Figure 4. Nuclear Overhauser effect (NOE) peaks. Summary of NOE data used to obtain sequence specific assignments. The line thickness is proportional to the observed cross-peak intensity. The chemical shift index is also plotted. The sequence is shown at the top of the figures with the secondary structure and disulfide bridges. The total number of NOEs per residue is plotted at the bottom of the figure: white for intraresidual, gray for sequential, dark gray for distances between 5 and 2 Å, and black for long-range distances of ≥5 Å.

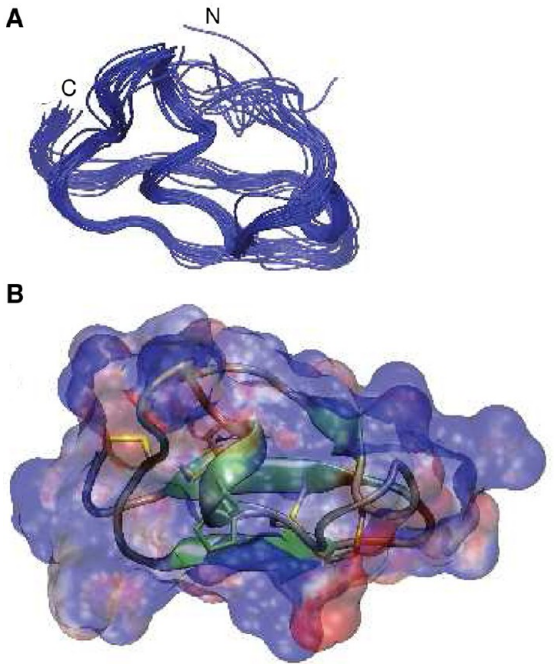

Figure 5. Three-dimensional (3D) structure. (A) Superposition of the 20 structures of Vm24. Twenty structures of 200 calculations are superimposed and plotted. The N- and C-terminal amino acids are denoted. The β-sheet is in the bottom part of the figure and the α-helix in the front. Although the N-terminal segment is not well-resolved because of the absence of NOEs, the backbone atoms of secondary structure elements show an rmsd of 0.442 Å. (B) Diagram of the 3D structure and potential surface. The 3D structure diagram is shown embedded in the electrostatic potential surface; the disulfide bridges are colored yellow. Prolines are drawn. The orientation of the protein is the same as in panel A. The N- and C-terminal residues are denoted. This folding is distinctive compared to those of other known peptides, mainly because of the short α-helix and the flat surface of the β-sheets.

mirrored in its pharmacological properties. The potency of the toxin in inhibiting potassium channels was tested on the human Kv1.3 channels, which are candidates for targeting with blockers for therapeutic applications. Figure 6 shows whole-cell K^+ currents recorded in human T lymphocytes. The standard voltage protocol for evoking voltage-gated Kv1.3-mediated K^+ currents consisted of a series of depolarizations to 50 mV from a holding potential of −120 mV. The time between voltage pulses was set to at least 15 s to prevent cumulative inactivation of Kv1.3 channels. Under the experimental conditions applied [the lack of Ca^{2+} in the pipet-filling solution and the nature of the voltage protocol (detailed in Materials and Methods and the figure legends)] the whole-cell currents were conducted exclusively by Kv1.3 channels.[53] Figure 6A displays macroscopic K^+ currents through Kv1.3 channels recorded sequentially in the same cell, before (control trace) and after the addition of 3 pM native Vm24 (nVm24) to the external solution by perfusion. Approximately two-thirds of the Kv1.3 current was inhibited in the presence of 3 pM Vm24. Washing the perfusion chamber with a toxin-free solution for several minutes resulted in no significant amount of current recovery (not shown). Figure 6B shows a similar experiment, except the synthetic peptide (sVm24) was applied at a concentration of 3 pM. sVm24 produced a block qualitatively similar to that of nVm24, but with a slightly stronger inhibition. The potency of native Vm24 and synthetic Vm24 to inhibit Kv1.3 channels was compared via the construction of dose−response relationships. The remaining current fraction (RCF = I/I_0, where I_0 and I are the peak currents in the absence and presence of the peptide, respectively, recorded at block saturation) was plotted at various concentrations for both toxins, and data points were fit by the Hill function to obtain K_d values. Figure 6C shows that the native and synthetic peptides have very similar effects, the synthetic toxin being slightly more potent (K_d = 0.5 pM) than the native peptide (K_d = 2.9 pM). Comparison of the blocking effects at different concentrations reveals significant differences at 1 and 3 pM, but not at 10 pM ($p < 0.057$) or 30 pM ($p < 0.112$). At a higher concentration (100 pM) of the peptides, block developed more quickly and more than 90% inhibition of the current was achieved for both nVm24 and sVm24 (for nVm24, RCF = 0.067 ± 0.03, and for sVm24, RCF = 0.085 ± 0.02; $p = 0.57$; $n \geq 4$). The 6-fold difference between the estimated K_d of synthetic and native peptides is likely due to inherent difficulties in the accurate determination of K_d because of the very slow k_{on} and k_{off} kinetics (see Native vs synthetic Vm24 in the Supporting Information).

An ion channel blocker of very high potency might influence not only the Kv1.3 K^+ channels of lymphocytes but also other ion channels, thereby leading to off-target toxic effects. We tested whether this was the case in a mouse model using the whole venom as well as the purified peptide. Mice treated with

dx.doi.org/10.1021/bi300060n | *Biochemistry* 2012, 51, 4049−4061

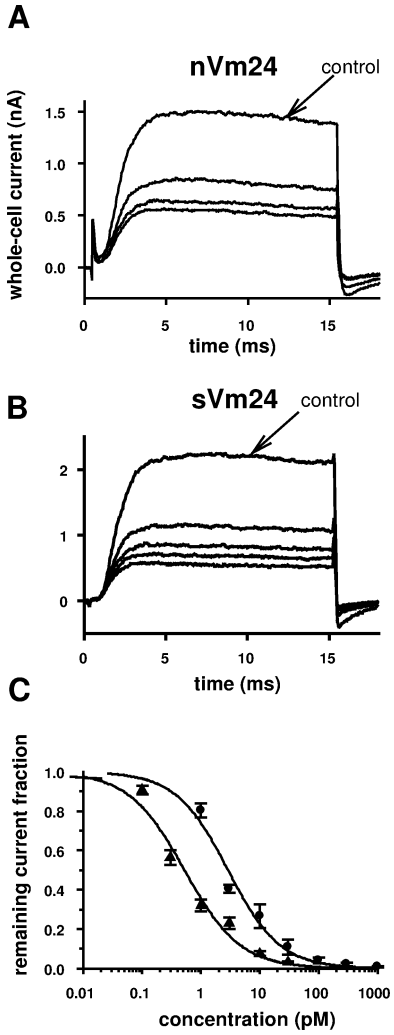

Figure 6. High-affinity block of hKv1.3 channels by native and synthetic Vm24. Whole-cell potassium currents through hKv1.3 channels were evoked from a human T cell in response to depolarizing pulses to 50 mV from a holding potential of −20 mV every 30 s. Currents recorded in the absence of the peptide (control) are substantially blocked when 3 pM natural [nVm24 (A)] or 3 pM synthetic Vm24 [sVm24 (B)] is administered to the cell via the perfusion of the extracellular medium. Traces recorded every 3 min following the application of the toxins are shown for the sake of clarity until equilibrium block was reached. (C) Dose−response relationship for both toxins obtained by plotting the remaining current fraction (RCF = I/I_0) as a function of toxin concentration, where I and I_0 are the peak currents measured in the presence and absence of the toxin, respectively, and fitting the data points with the function RCF = $K_d^n/(K_d^n + [\mathrm{Tx}]^n)$, where [Tx] indicates the toxin concentration and K_d is the dissociation constant. Error bars indicate the SEM (n = 3−7). The dose−response function constructed in this way yields K_d values of 2.9 and 0.5 pM for nVm24 and sVm24, respectively, and Hill coefficients (n) of ∼1 for both toxins.

various amounts of *Vm smithi* soluble venom [from 50 to 200 μg of protein per mouse (20 g body weight)] showed no symptoms of intoxication. Although the whole venom is not toxic, a purified peptide at similar doses can induce symptoms of intoxication, because during purification the sample is enriched in that particular component. For this reason, pure Vm24 was injected into mice at doses comparable to that of the whole venom (50−200 μg/20 g of mouse weight). Even at the highest dose of 200 μg/20 g (corresponding to 10 mg/kg of mouse weight), the pure peptide evoked no symptoms of intoxication.

Phylogenetic Analysis and a New Subfamily. Among the top-10 BLAST[54] hits of Vm24 against the nr database, three sequences each from α-KTx subfamilies 3, 4, and 6 were retrieved, although with poor expectation values (10^{-4}−10^{-1}). Closer inspection against all short chain toxins reported to date suggests that Vm24 could be classified as a new member of α-KTx subfamily 4 or 6 (following the proposal of ref 6). Pairwise comparison, however, reveals a low level of identity with other members of both subfamilies. To clarify the relationship of Vm24 with the entire α-KTx family, Bayesian phylogenetic inference analysis was performed as described previously[18] with MrBayes version 3.1.2,[19,20] using the multiple-sequence alignment of 101 α-KTx sequences. This reconstruction shows that α-KTx subfamilies 6 and 7 segregate, in 97% of the final tree set, as a monophyletic group. The analysis also places Vm24 as a sister group of this clade in 98% of the final tree set (Figure 7B), which strongly supports the classification of Vm24 as a novel α-KTx subfamily. We propose that Vm24 is the first example of a new subfamily, whose systematic number should be α-KTx 23.1 (but see A note on systematic nomenclature of Vm24 in the Supporting Information).

Molecular Docking. Pore-blocking animal toxins are known to interact with Kv1.*x*, KCa1.1, and KCa3.1 with a similar pharmacophore, dubbed the "functional dyad",[55] formed by a pore-plugging lysine and an aromatic side chain located within ∼7 Å of each other.[56] The three-dimensional structure of Vm24 reveals a dyadlike arrangement of K25 and Y34 (average distance between side chain atoms of ∼6 Å), so we hypothesize that Vm24 interacts with Kv1.3 with the pore-blocking mode of α-KTx.[57] To rationalize the striking specificity of Vm24, we modeled its interaction with Kv1.3 channels by molecular docking, conducted on the RosettaDock server. Three well-populated interaction modes were retrieved (not shown), with two of them displaying the critical Lys25 making contacts with the channel's selectivity filter and Tyr35 making extensive contacts with the bottom of the vestibule. In the remaining mode, the toxin is tilted on the turrets, in a nonblocking fashion. A more in-depth analysis revealed that in both pore-blocking modes the toxin is superimposable if the tetrameric nature of the channel is taken into consideration, so we regard them as a single interaction mode. The rmsf for individual residues among the 20 top-scoring pore-blocking complexes ranges from 2.5 Å for the β-hairpin residues to 7.5 Å for the residues preceding the α-helix (Figure 8A). In this interaction mode, the toxin docks deeply into the channel mouth, in a slightly lateral fashion (Figure 8B). In panels B (channel) and C (toxin) of Figure 8, residues making intermolecular contacts in at least 50% of the final ensemble are color-coded according to their prevalence. Statistical comparison of pore-blocking mode with the rest of the docking solutions revealed significant differences in terms of both the docking score and the number of contacts, with pore-plugging complexes having better scores (more negative values in Rosetta terms) and >1.5-fold times more contacts than nonblocking complexes (in a two-tailed Kolmogorov−Smirnov test, $p < 2 \times 10^{-16}$ for both comparisons).

The same differences between pore-blocking and non-blocking docking configurations were obtained with ADWX-1[38] and Mokatoxin,[15] two recently described high-affinity α-KTx-like Kv1.3 blockers, when analyzed by the same procedure (not shown). To further support the discrimination obtained

dx.doi.org/10.1021/bi300060n | *Biochemistry* 2012, 51, 4049−4061

A

```
                                                                %I   RMSD/L   Kd      Refs
P0DJ31|2k9o|Vm24          --AAAISCVGSPSCPPKCRAQ-GCKNG-KCMNRKCKCYYC   -    -        0.003   this report
P13487|2crd|ChTx α1.1     -QFTNVSCTTSKECWSVCQRLHNTSRG-KCMNKKCRCYS-   42   2.33/30  3.5     (65)
P24663|n.a.|IbTx α1. 3    -QFTDVDCSVSKECWSVCKDLFGVDRG-KCMGKKCRCYQ-   39   n.a.     -       (64)
P08815|1sxm|NTx α2.1      -TIINVKCTSPKQCSKPCKELYGSSAGAKCMNGKCKCYNN   31   2.41/32  0.25    (66)
P24662|1ktx|KTx α3.1      GVEINVKCSGSPQCLKPCKDA-GMRFG-KCMNRKCHCTPK   39   3.65/24  0.41    (67)
P46114|1hp2|TsKα α4.1     -VFINAKCRGSPECLPKCKEAIGKAAG-KCMNGRCKCYP-   53   3.05/33  3.9     (68)
P80719|1txm|MauTx α6.2    -----VSCTGSKDCYAPCRKQTGCPNA-KCINKSCKCYGC   39   2.22/26  -       (69)
P59867|1qux|HsTx1 α6.3    -----ASCRTPKDCADPCRKETGCPYG-KCMNRKCKCNRC   47   2.41/26  0.012   (70)
synthe|2ck4|[K16,D20]OSK1 GVIINVKCKISRQCLEPCKKA-GMRFG-KCMNGKCHCTPK   36   2.99/34  0.003   (9)
synthe|2k4u|ADWX-1        -VGINVKCKHSRQCLKPCKDA-GMRFG-KCTNGKCHCTPK   33   2.73/32  0.002   (10)
synthe|2kir|Mokatoxin     ---INVKCSLPQQCIKPCKDA-GMRFG-KCMNKKCRCYS-   36   2.25/24  1.0     (15)
```

B

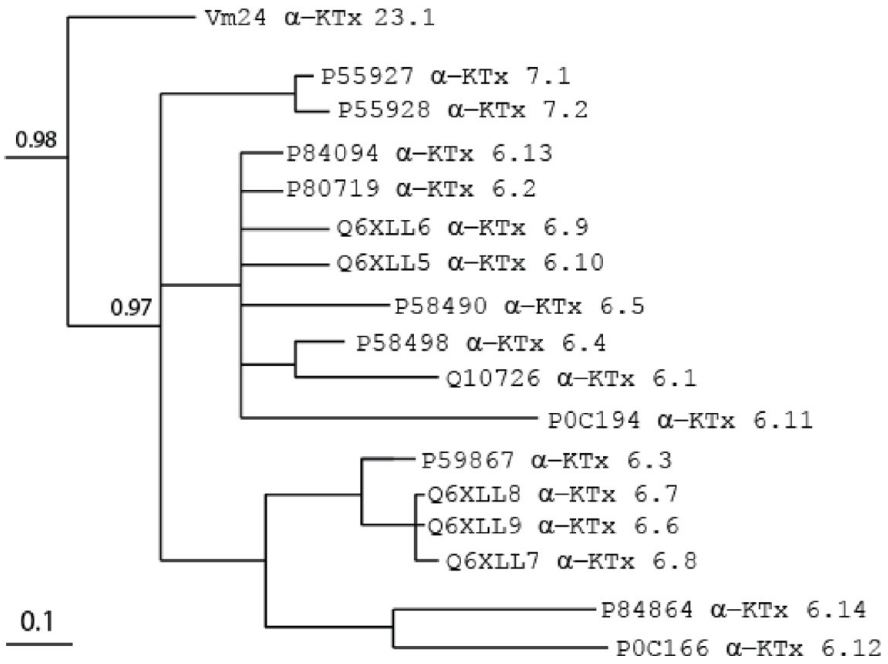

Figure 7. Sequence comparison and phylogenetic reconstruction. (A) Multiple-sequence alignment of Vm24 with selected α-KTx peptides. The alignment was performed with CLUSTAL_X.[17] rmsd values were obtained with the longest alignment in pairwise TopMatch.[37] K_d values of the selected peptides against Kv1.3 were taken from refs 3, 9, 10, and 15 Sequences are named by their UniProt codes, PDB codes, trivial names, and systematic numbering where available. Abbreviations: %I, percentage identity; L, length of the structural alignment; n.a., not available; synthe, synthetic construct. Dots above the alignment denote residues discussed in the text. Residues colored red are those making contact with the channel according to the references provided in the last column. "Functional dyad" residues are underlined. Shaded residues indicate the positions of Vm24 matched in at least three of the other toxins shown.[66,67,69] (B) Pruned phylogenetic tree reconstructed with MrBayes version 3.1.2.[19,20] Vm24 segregates as a sister group of subfamilies α-KTx 6 and 7.

by RosettaDock, a cross-referenced analysis of the interaction of Maurotoxin, an α-KTx known to interact tightly with KCa3.1 channels and only poorly with Kv1.3 channels,[58] was conducted. Reciprocally, the pore-blocking configuration reaches better docking scores than the nonblocking ones, while displaying a significantly larger number of contacts with KCa3.1. Moreover, statistical discrimination values between distributions are consistently better for the case of the Maurotoxin−KCa3.1 interaction than a control docking of Maurotoxin and Kv1.3 channels (not shown).

DISCUSSION

Scorpion toxins classified within the α-KTx family are among the best known peptide blockers of K^+ channels. All the members of this family are structurally related and perform functions similar to those of potassium channel blockers; nonetheless, they display variable selectivity for certain types and subtypes of potassium channels.[4] The rationale followed by the international panel of experts that proposed the classification was that a given subfamily could be identified by a high percentage of similarity among its members and a low level of identity with members of other subfamilies.[6] It has been demonstrated that this distinction mirrored, to some extent, the pharmacological spectrum of most subfamilies.[4,59] Hence, if the relatively restricted variability of the family, because of its reduced size, is taken into consideration, it is important to identify the molecular and structural characteristics that confer a given functional spectrum. On the basis of the phylogenetic reconstruction implemented here and the guidelines suggested by an international panel of experts,[6] it is clear that Vm24 defines a novel subfamily of scorpion toxins that recognize K^+ channels; thus, its systematic numbering should be α-KTx 23.1 (see further discussion in the Supporting Information). The electrophysiological experiments clearly demonstrated that both Vm24 and sVm24 reduce the peak Kv1.3 current at low picomolar concentrations (see also further discussion in the Supporting Information). The inhibition of the current is attributed to block of Kv1.3 channels by Vm24 as demonstrated by the analysis of the kinetics of current inhibition, the mutually exclusive binding of the well-known K^+-channel blocker ChTx

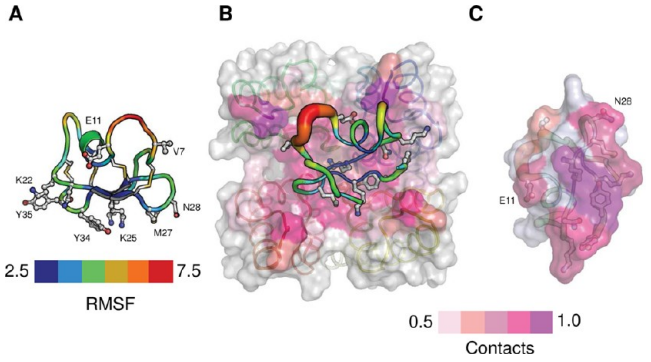

Figure 8. Computational model of the Vm24–Kv1.3 interaction. (A) Three-dimensional structure of Vm24 highlighting interacting residues (balls and sticks) and rmsfs over the 20 top-scoring complexes in the pore-blocking mode. (B) Pore-blocking mode of Vm24 on Kv1.3. The toxin backbone is displayed proportionally to the rmsf. The channel surface is colored according to the number of contacts verified in the pore-blocking mode (color code below). (C) Molecular surface of Vm24 highlighting interacting residues color-coded as described above.

and Vm24 to the external vestibule of the channel, and the lack of off-target effects of Vm24 (Z. Varga, G. Gurrola-Briones, F. Papp, R.C. Rodríguez de la Vega, G. Pedraza-Alva, R.B. Tajhya, R. Gáspár, L. Cardenas, Y. Rosenstein, C. Beeton, L.D. Possani, G. Panyi, manuscript submitted to Molecular Pharmacology for publication).

Purified Vm24 injected intraperitoneally at doses of up to 200 μg/20 g of mouse weight produced no symptoms of intoxication (~50 μM assuming a homogeneous distribution in a total extracellular volume of 1 mL for a 20 g body weight). This is in sharp contrast with other known scorpion K^+ channel toxins, such as Noxiustoxin, which is deadly at doses of 40 μg/20 g of mouse body weight.[60] Taking into consideration the fact that the physiological modifications of K^+ currents in human lymphocytes were observed at low picomolar concentrations, we think it is reasonable to assume that pharmacological doses of Vm24 will be nontoxic to humans.

At the sequence level, the most obvious difference between Vm24 and the dozens of known α-KTx peptides resides at its N-terminus (Figure 7A), which adopts a unique three-dimensional structure, including an extra β-strand and a loosely defined α-helix segment (Figure 5). For the pore-blocking mode of α-KTx, it is assumed that the main determinants of the interaction reside on the C-terminal β-hairpin, including the functional dyad residues, with the distinct assistance of surrounding residues.[56] This region is also the most conserved among pore-blocking α-KTx (see Figure 7A); thus, it would be hard to explain the remarkable selectivity of Vm24 for Kv1.3 channels on the basis of only this region. Molecular docking suggests a likely explanation: the Vm24 N-terminal segment (residues A1–E11) makes extensive contacts with the channel (median of 11 intermolecular contacts among complexes in the pore-blocking mode). Strikingly, the nonconserved E11 in the toxin contacts the also nonconserved H451 in the channel (Figure 8B and not shown, UniProt entry P22001); this position has been highlighted as critically defining the affinity of a number of blocking toxins for Kv1 channels.[61] The large number of contacts made by the channel's turret residues is also worth noting in this respect (Figure 8B); residues in this variable region have been implicated in the selectivity of α-KTx toward Kv1.*x* and KCa1.1 channels,[62] particularly because of contacts with the residues homologous to Vm24 N28 in AgTx2, N30,[63] and IbTx, G30[64] (also see Figure 7A). In a control docking between Vm24 and KCa3.1, this specific pair was found to make contacts in <15% of the 1000 models (not shown). Taken together, these comparisons suggest that E11 and N28 contribute to the remarkable Kv1.3 specificity of Vm24.

The molecular determinants for the interaction between α-KTx and Kv1.3 channels have been extensively studied by means of double-mutant cycles, molecular docking, and even the direct determination of intermolecular NMR couplings for a toxin–channel complex (references in Figure 7A). Besides the functional dyad residues, only the homologous positions of Vm24's M27 and N28 have been consistently found to be in contact with the channel. That fact notwithstanding, positions preceding the α-helix have been identified as being important for Kv1.3 blockade in all the sequences presented in Figure 7A. It almost goes without saying that residues in this region contact the nonconserved turrets of K^+ channels.[9,10,65,68,70] Our own docking results follow the line of these previous findings, pointing to an important contribution of nonconserved residues, those before the α-helix in the scorpion venom peptides, in defining the specificity of the interaction toward the binding to the most variable region in the receptor, the turret. The most conserved region of α-KTx, the β-hairpin, in turn targets the largely conserved bottom of the channel's vestibule. Thus, it seems that there were two "pharmacophores", one defining the blockade and the other the specificity.

The very high affinity of Vm24 for Kv1.3 serves as a basis for its therapeutic potential in the management of autoimmune diseases in which tissue-infiltrating T_{EM} cells are implicated in the pathogenesis. The proliferation of T_{EM} cells is Kv1.3-dependent, which is manifested in a persistent inhibition of T_{EM} cell proliferation in the presence of high-affinity Kv1.3 inhibitors. Vm24, in addition to its high Kv1.3 affinity, also exhibits ~1500-fold selectivity for Kv1.3 over 10 other ion channels tested, with blocking potency decreasing in the following order: hKv1.3 $\gg$ hKv1.2 > hKCa3.1 > mKv1.1 $\gg$ hKv1.4 $\approx$ hKv1.5 $\approx$ rKv2.1 $\approx$ hKv11.1 $\approx$ hKCa1.1 $\approx$ hKCa2.3 $\approx$ hNaV1.5 (Z. Varga, G. Gurrola-Briones, F. Papp, R.C. Rodríguez de la Vega, G. Pedraza-Alva, R.B. Tajhya, R. Gáspár, L. Cardenas, Y. Rosenstein, C. Beeton, L.D. Possani, G. Panyi, manuscript submitted to Molecular Pharmacology for publication). This confers upon the peptide the capacity for specific immune suppression, i.e., inhibiting autoimmune reactions without compromising more immediate immune responses. The latter is based on the upregulation of the KCa3.1 channel expression of activated naïve and central memory T cells, thus rendering the proliferation of these cells insensitive to Kv1.3 blockage. Because of the unique molecular and pharmacological properties of Vm24, this molecule may thus serve as an invaluable tool in targeting Kv1.3 channels and the physiological/pathophysiological responses depending on Kv1.3 activity.

■ ASSOCIATED CONTENT

Supporting Information

Proteomic analysis of *Vm smithi* soluble venom (Table S1), CYNA data analysis (Table S2), rmsds for the final structural ensemble (Table S3), Ramachandran plot (Figure S1), supplementary discussion of native versus synthetic Vm24, a note on the systematic nomenclature of Vm24, and additional

references. This material is available free of charge via the Internet at http://pubs.acs.org.

Accession Codes

NMR assignment data and atomic coordinates of Vm24 have been deposited in BioMagResBank (entry 15992) and the Protein Data Bank (entry 2k9o). The amino acid sequence was deposited in UniProt (entry P0DJ31).

AUTHOR INFORMATION

Corresponding Author

*Phone: +52-77-73171209. Fax: +52-77-73172388. E-mail: possani@ibt.unam.mx.

Present Address

[@]Department of Chemistry and Chemical Biology, Harvard University, Cambridge, MA 02138.

Funding

This work was partially supported by the Consejo Nacional de Ciencia y Tecnologia (CONACyT), Mexican Government (Grants SEP153496 to L.D.P. and 59297 to F.d.R.-P.), Dirección General de Asuntos del Personal Académico (DGAPA)-UNAM numbers IN204110 to L.D.P. and IN213807 to F.d.R.-P., and Dirección General de Computo Académico-UNAM. It was also supported by Grants OTKA CK 78179 and Tásadalmi Megújulás Operatív Program-TÁMOP 4.2.2-08/1/2008-0019, and TÁMOP-4.2.1/B-09/1/KONV-2010-007 to G.P. The bilateral collaboration CONACyT and the Hungarian Science Fund is gratefully acknowledged. The research of R.C.R.d.l.V. is funded by the European Union Seventh Framework Programme (FP7/2007-2013) under Grant 246556.

Notes

The authors declare no competing financial interest.

A patent related to Vm24 inhibition of Kv1.3 channels was filed and published by the International Bureau of the World Intellectual Property Organization as Patent WO 20087139243 (A1).

ACKNOWLEDGMENTS

The technical assistance of Mario Trejo, Dr. Fernando Z. Zamudio, Elizabeth Mata, Erika Melchy, and C. Nagy is acknowledged.

ABBREVIATIONS

DQ-COSY, double-quantum-correlated spectroscopy; Kv1.3, voltage-dependent K^+ channel, subtype 1.3; MD, molecular dynamics; NMR, nuclear magnetic resonance; NOE, nuclear Overhauser effect; NOESY, NOE spectroscopy; TOCSY, total correlation spectroscopy; *NVT*, isochromic isothermal ensemble for the number of particles, volume, and temperature; *NPT*, isobaric isothermal ensemble for the number of particles, pressure, and temperature; T_{EM}, effector memory T cells; rmsd, root-mean-square deviation; rmsf, root-mean-square fluctuation.

REFERENCES

(1) Cahalan, M. D., and Chandy, K. G. (2009) The functional network of ion channels in T lymphocytes. *Immunol. Rev. 231*, 59−87.

(2) Beeton, C., Wulff, H., Standifer, N. E., Azam, P., Mullen, K. M., Pennington, M. W., Kolski-Andreaco, A., Wei, E., Grino, A., Counts, D. R., Wang, P. H., Leehealey, C. J., Andrews, S., Sankaranarayanan, A., Homerick, D., Roeck, W. W., Tehranzadeh, J., Stanhope, K. L., Zimin, P., Havel, P. J., Griffey, S., Knaus, H. G., Nepom, G. T., Gutman, G. A., Calabresi, P. A., and Chandy, K. G. (2006) Kv1.3 channels are a therapeutic target for T cell-mediated autoimmune diseases. *Proc. Natl. Acad. Sci. U.S.A. 103*, 17414−17419.

(3) Panyi, G., Possani, L. D., Rodríguez de la Vega, R. C., Gaspar, R., and Varga, Z. (2006) K^+ channel blockers: Novel tools to inhibit T cell activation leading to specific immunosuppression. *Curr. Pharm. Des. 12*, 2199−2220.

(4) Rodríguez de la Vega, R. C., and Possani, L. D. (2004) Current views on scorpion toxins specific for K^+-channels. *Toxicon 43*, 865−875.

(5) Miller, C. (1995) The Charybdotoxin family of K^+-channel-blocking peptides. *Neuron 15*, 5−10.

(6) Tytgat, J., Chandy, K. G., Garcia, M. L., Gutman, G. A., Martin-Eauclaire, M. F., van der Walt, J. J., and Possani, L. D. (1999) A unified nomenclature for short-chain peptides isolated from scorpion venoms: α-KTx molecular subfamilies. *Trends Pharmacol. Sci. 20*, 444−447.

(7) Jungo, F., Bougueleret, L., Xenarios, I., and Poux, S. (2012) The UniProtKB/Swiss-Prot Tox-Prot program: A central hub of integrated venom protein data. *Toxicon*, DOI 10.1016/j.toxicon.2012.03.10.

(8) Giangiacomo, K. M., Ceralde, Y., and Mullmann, T. J. (2004) Molecular basis of α-KTx specificity. *Toxicon 43*, 877−886.

(9) Mouhat, S., Visan, V., Ananthakrishnan, S., Wulff, H., Andreotti, N., Grissmer, S., Darbon, H., De Waard, M., and Sabatier, J. M. (2005) K^+ channel types targeted by synthetic OSK1, a toxin from *Orthochirus scrobiculosus* scorpion venom. *Biochem. J. 385*, 95−104.

(10) Han, S., Yi, H., Yin, S. J., Chen, Z. Y., Liu, H., Cao, Z. J., Wu, Y. L., and Li, W. X. (2008) Structural basis of a potent peptide inhibitor designed for Kv1.3 channel, a therapeutic target of autoimmune disease. *J. Biol. Chem. 283*, 19058−19065.

(11) Castaneda, O., Sotolongo, V., Amor, A. M., Stocklin, R., Anderson, A. J., Harvey, A. L., Engstrom, A., Wernstedt, C., and Karlsson, E. (1995) Characterization of a potassium channel toxin from the caribbean sea anemone *Stichodactyla helianthus*. *Toxicon 33*, 603−613.

(12) Pennington, M. W., Byrnes, M. E., Zaydenberg, I., Khaytin, I., de Chastonay, J., Krafte, D. S., Hill, R., Mahnir, V. M., Volberg, W. A., Gorczyca, W., and Kem, W. R. (1995) Chemical synthesis and characterization of ShK toxin: A potent potassium channel inhibitor from a sea anemone. *Int. J. Pept. Protein Res. 46*, 354−358.

(13) Kalman, K., Pennington, M. W., Lanigan, M. D., Nguyen, A., Rauer, H., Mahnir, V., Paschetto, K., Kem, W. R., Grissmer, S., Gutman, G. A., Christian, E. P., Cahalan, M. D., Norton, R. S., and Chandy, K. G. (1998) ShK-Dap22, a potent Kv1.3-specific immunosuppressive polypeptide. *J. Biol. Chem. 273*, 32697−32707.

(14) Pennington, M. W., Beeton, C., Galea, C. A., Smith, B. J., Chi, V., Monaghan, K. P., Garcia, A., Rangaraju, S., Giuffrida, A., Plank, D., Crossley, G., Nugent, D., Khaytin, I., Lefievre, Y., Peshenko, I., Dixon, C., Chauhan, S., Orzel, A., Inoue, T., Hu, X., Moore, R. V., Norton, R. S., and Chandy, K. G. (2009) Engineering a stable and selective peptide blocker of the Kv1.3 channel in T lymphocytes. *Mol. Pharmacol. 75*, 762−773.

(15) Takacs, Z., Toups, M., Kollewe, A., Johnson, E., Cuello, L. G., Driessens, G., Biancalana, M., Koide, A., Ponte, C. G., Perozo, E., Gajewski, T. F., Suarez-Kurtz, G., Koide, S., and Goldstein, S. A. (2009) A designer ligand specific for Kv1.3 channels from a scorpion neurotoxin-based library. *Proc. Natl. Acad. Sci. U.S.A. 106*, 22211−22216.

(16) Batista, C. V., Roman-Gonzalez, S. A., Salas-Castillo, S. P., Zamudio, F. Z., Gomez-Lagunas, F., and Possani, L. D. (2007) Proteomic analysis of the venom from the scorpion *Tityus stigmurus*: Biochemical and physiological comparison with other tityus species. *Comp. Biochem. Physiol., Part C: Toxicol. Pharmacol. 146*, 147−157.

(17) Larkin, M. A., Blackshields, G., Brown, N. P., Chenna, R., McGettigan, P. A., McWilliam, H., Valentin, F., Wallace, I. M., Wilm, A., Lopez, R., Thompson, J. D., Gibson, T. J., and Higgins, D. G. (2007) Clustal W and Clustal X version 2.0. *Bioinformatics 23*, 2947−2948.

(18) Bagdany, M., Batista, C. V., Valdez-Cruz, N. A., Somodi, S., Rodríguez de la Vega, R. C., Licea, A. F., Varga, Z., Gaspar, R., Possani,

L. D., and Panyi, G. (2005) Anuroctoxin, a new scorpion toxin of the α-KTx 6 subfamily, is highly selective for Kv1.3 over IKCa1 ion channels of human T lymphocytes. *Mol. Pharmacol. 67*, 1034−1044.
(19) Huelsenbeck, J. P., and Ronquist, F. (2001) MRBAYES: Bayesian inference of phylogenetic trees. *Bioinformatics 17*, 754−755.
(20) Ronquist, F., and Huelsenbeck, J. P. (2003) MrBayes 3: Bayesian phylogenetic inference under mixed models. *Bioinformatics 19*, 1572−1574.
(21) Sarin, V. K., Kent, S. B., Tam, J. P., and Merrifield, R. B. (1981) Quantitative monitoring of solid-phase peptide synthesis by the ninhydrin reaction. *Anal. Biochem. 117*, 147−157.
(22) King, D. S., Fields, C. G., and Fields, G. B. (1990) A cleavage method which minimizes side reactions following Fmoc solid phase peptide synthesis. *Int. J. Pept. Protein Res. 36*, 255−266.
(23) Delaglio, F., Grzesiek, S., Vuister, G. W., Zhu, G., Pfeifer, J., and Bax, A. (1995) NMRPIPE: A multidimensional spectral processing system based on UNIX pipes. *J. Biomol. NMR 6*, 277−293.
(24) Bartels, C., Xia, T., Billeter, M., Guntert, P., and Wutrich, K. (1995) The program XEASY for computer-supported NMR spectral analysis of biological macromolecules. *J. Biomol. NMR 5*, 1−10.
(25) Wagner, G., and Wuthrich, K. (1982) Sequential resonance assignments in protein ^{1}H nuclear magnetic resonance spectra. Basic pancreatic trypsin inhibitor. *J. Mol. Biol. 155*, 347−366.
(26) Piantini, U., Sorensen, O. W., and Ernst, R. R. (1982) Multiple quantum filters for elucidating NMR coupling networks. *J. Am. Chem. Soc. 104*, 6800−6801.
(27) Braunschweiler, L., and Ernst, R. R. (1983) Coherence transfer by isotropic mixing: Application to proton correlation spectroscopy. *J. Magn. Reson. 53*, 521−528.
(28) Jeener, J., Meier, M. H., Bachmann, P., and Ernst, R. R. (1979) Investigation of exchange processes by two-dimensional NMR spectroscopy. *J. Chem. Phys. 71*, 4546−4553.
(29) Guntert, P., Mumenthaler, C., and Wuthrich, K. (1997) Torsion angle dynamics for NMR structure calculation with the new program DYANA. *J. Mol. Biol. 273*, 283−298.
(30) Herrmann, T., Guntert, P., and Wuthrich, K. (2002) Protein NMR structure determination with automated NOE-identification in the NOESY spectra using the new software ATNOS. *J. Biomol. NMR 24*, 171−189.
(31) Case, D. A., Cheatham, T. E., III, Darden, T., Gohlke, H., Luo, R., Merz, K. M., Jr., Onufriev, A., Simmerling, C., Wang, B., and Woods, R. J. (2005) The Amber biomolecular simulation programs. *J. Comput. Chem. 26*, 1668−1688.
(32) Hornak, V., Abel, R., Okur, A., Strockbine, B., Roitberg, A., and Simmerling, C. (2006) Comparison of multiple Amber force fields and development of improved protein backbone parameters. *Proteins 65*, 712−725.
(33) Xia, B., Tsui, V., Case, D. A., Dyson, H. J., and Wright, P. E. (2002) Comparison of protein solution structures refined by molecular dynamics simulation in vacuum, with a generalized Born model, and with explicit water. *J. Biomol. NMR 22*, 317−331.
(34) Deutsch, C., Krause, D., and Lee, S. C. (1986) Voltage-gated potassium conductance in human T lymphocytes stimulated with phorbol ester. *J. Physiol. 372*, 405−423.
(35) Matteson, D. R., and Deutsch, C. (1984) K channels in T lymphocytes: A patch clamp study using monoclonal antibody adhesion. *Nature 307*, 468−471.
(36) Hamill, O. P., Marty, A., Neher, E., Sakmann, B., and Sigworth, F. J. (1981) Improved patch-clamp techniques for high-resolution current recording from cells and cell-free membrane patches. *Pfluegers Arch. 391*, 85−100.
(37) Sippl, M. J., and Wiederstein, M. (2008) A note on difficult structure alignment problems. *Bioinformatics 24*, 426−427.
(38) Yin, S. J., Jiang, L., Yi, H., Han, S., Yang, D. W., Liu, M. L., Liu, H., Cao, Z. J., Wu, Y. L., and Li, W. X. (2008) Different residues in channel turret determining the selectivity of ADWX-1 inhibitor peptide between Kv1.1 and Kv1.3 channels. *J. Proteome Res. 7*, 4890−4897.
(39) Blanc, E., Sabatier, J. M., Kharrat, R., Meunier, S., El Ayeb, M., Van Rietschoten, J., and Darbon, H. (1997) Solution Structure of Maurotoxin, a scorpion toxin from *Scorpio maurus*, with high affinity for voltage-gated potassium channels. *Proteins 29*, 321−333.
(40) Lyskov, S., and Gray, J. J. (2008) The RosettaDock server for local protein-protein docking. *Nucleic Acids Res. 36*, W233−W238.
(41) Chen, X., Wang, Q., Ni, F., and Ma, J. (2010) Structure of the full-length Shaker potassium channel Kv1.2 by normal-mode-based X-ray crystallographic refinement. *Proc. Natl. Acad. Sci. U.S.A. 107*, 11352−11357.
(42) Bordoli, L., Kiefer, F., Arnold, K., Benkert, P., Battey, J., and Schwede, T. (2009) Protein structure homology modeling using SWISS-MODEL workspace. *Nat. Protoc. 4*, 1−13.
(43) Krissinel, E., and Henrick, K. (2007) Inference of macromolecular assemblies from crystalline state. *J. Mol. Biol. 372*, 774−797.
(44) Eswar, N., Webb, B., Marti-Renom, M. A., Madhusudhan, M. S., Eramian, D., Shen, M. Y., Pieper, U., and Sali, A. (2007) Comparative protein structure modeling using modeller. *Current Protocols in Protein Science*, Chapter 2, Unit 2.9, Wiley, New York.
(45) Corzo, G., Papp, F., Varga, Z., Barraza, O., Espino-Solis, P. G., Rodríguez de la Vega, R. C., Gaspar, R., Panyi, G., and Possani, L. D. (2008) A selective blocker of Kv1.2 and Kv1.3 potassium channels from the venom of the scorpion *Centruroides suffusus suffusus*. *Biochem. Pharmacol. 76*, 1142−1154.
(46) Gray, J. J., Moughon, S., Wang, C., Schueler-Furman, O., Kuhlman, B., Rohl, C. A., and Baker, D. (2003) Protein-protein docking with simultaneous optimization of rigid-body displacement and side-chain conformations. *J. Mol. Biol. 331*, 281−299.
(47) Yu, L., Sun, C., Song, D., Shen, J., Xu, N., Gunasekera, A., Hajduk, P. J., and Olejniczak, E. T. (2005) Nuclear magnetic resonance structural studies of a potassium channel-Charybdotoxin complex. *Biochemistry 44*, 15834−15841.
(48) DeLano, W. L. (2002) *The PyMOL Molecular Graphics System*, DeLano Scientific, San Carlos, CA.
(49) Nascimento, D. G., Rates, B., Santos, D. M., Verano-Braga, T., Barbosa-Silva, A., Dutra, A. A., Biondi, I., Martin-Eauclaire, M. F., De Lima, M. E., and Pimenta, A. M. (2006) Moving pieces in a taxonomic puzzle: Venom 2D-LC/MS and data clustering analyses to infer phylogenetic relationships in some scorpions from the Buthidae family (Scorpiones). *Toxicon 47*, 628−639.
(50) Rodríguez de la Vega, R. C., Schwartz, E. F., and Possani, L. D. (2010) Mining on scorpion venom biodiversity. *Toxicon 56*, 1155−1161.
(51) Baker, N. A., Sept, D., Joseph, S., Holst, M. J., and McCammon, J. A. (2001) Electrostatics of nanosystems: Application to microtubules and the ribosome. *Proc. Natl. Acad. Sci. U.S.A. 98*, 10037−10041.
(52) Humphrey, W., Dalke, A., and Schulten, K. (1996) VMD: Visual molecular dynamics. *J. Mol. Graphics 14*, 33−38.
(53) Peter, M. J., Varga, Z., Hajdu, P., Gaspar, R. J., Damjanovich, S., Horjales, E., Possani, L. D., and Panyi, G. (2001) Effects of toxins Pi2 and Pi3 on human T lymphocyte Kv1.3 channels: The role of Glu7 and Lys24. *J. Membr. Biol. 179*, 13−25.
(54) Altschul, S. F., Gish, W., Miller, W., Myers, E. W., and Lipman, D. J. (1990) Basic Local Alignment Search Tool. *J. Mol. Biol. 215*, 403−410.
(55) Dauplais, M., Lecoq, A., Song, J., Cotton, J., Jamin, N., Gilquin, B., Roumestand, C., Vita, C., de Medeiros, C. L., Rowan, E. G., Harvey, A. L., and Menez, A. (1997) On the convergent evolution of animal toxins. Conservation of a diad of functional residues in potassium channel-blocking toxins with unrelated structures. *J. Biol. Chem. 272*, 4302−4309.
(56) Mouhat, S., De Waard, M., and Sabatier, J. M. (2005) Contribution of the functional dyad of animal toxins acting on voltage-gated Kv1-type channels. *J. Pept. Sci. 11*, 65−68.
(57) Rodríguez de la Vega, R. C., Merino, E., Becerril, B., and Possani, L. D. (2003) Novel interactions between K^+ channels and scorpion toxins. *Trends Pharmacol. Sci. 24*, 222−227.

(58) Visan, V., Fajloun, Z., Sabatier, J. M., and Grissmer, S. (2004) Mapping of maurotoxin binding sites on hKv1.2, hKv1.3, and hIKCa1 channels. *Mol. Pharmacol. 66*, 1103−1112.
(59) Zhu, S., Huys, I., Dyason, K., Verdonck, F., and Tytgat, J. (2004) Evolutionary trace analysis of scorpion toxins specific for K-channels. *Proteins 54*, 361−370.
(60) Gurrola, G. B., Molinar-Rode, R., Sitges, M., Bayon, A., and Possani, L. D. (1989) Synthetic peptides corresponding to the sequence of noxiustoxin indicate that the active site of this K^+-channel blocker is located on its amino-terminal portion. *J. Neural Transm. 77*, 11−20.
(61) Gilquin, B., Braud, S., Eriksson, M. A., Roux, B., Bailey, T. D., Priest, B. T., Garcia, M. L., Ménez, A., and Gasparini, S. (2005) A variable residue in the pore of Kv1 channels is critical for the high affinity of blockers from sea anemones and scorpions. *J. Biol. Chem. 280*, 27093−27102.
(62) Gao, Y. D., and Garcia, M. L. (2003) Interaction of Agitoxin2, Charybdotoxin, and Iberiotoxin with potassium channels: Selectivity between voltage-gated and maxi-K channels. *Proteins 52*, 146−154.
(63) Eriksson, M. A., and Roux, B. (2002) Modeling the structure of agitoxin in complex with the shaker K^+ channel: A computational approach based on experimental distance restraints extracted from thermodynamic mutant cycles. *Biophys. J. 83*, 2595−2609.
(64) Giangiacomo, K. M., Becker, J., Garsky, C., Felix, J. P., Priest, B. T., Schmalhofer, W., Garcia, M. L., and Mullmann, T. J. (2007) Revealing the molecular determinants of neurotoxin specificity for calcium-activated versus voltage-dependent potassium channels. *Biochemistry 46*, 5358−5364.
(65) Khabiri, M., Nikouee, A., Cwiklik, L., Grissmer, S., and Ettrich, R. (2011) Charybdotoxin unbinding from the mKv1.3 potassium channel: A combined computational and experimental study. *J. Phys. Chem. B 115*, 11490−11500.
(66) Yu, K., Fu, W., Liu, H., Luo, X., Chen, K. X., Ding, J., Shen, J., and Jiang, H. (2004) Computational simulations of interactions of scorpion toxins with the voltage-gated potassium ion channel. *Biophys. J. 86*, 3542−3555.
(67) Lange, A., Giller, K., Hornig, S., Martin-Eauclaire, M. F., Pongs, O., Becker, S., and Baldus, M. (2006) Toxin-induced conformational changes in a potassium channel revealed by solid-state NMR. *Nature 440*, 959−962.
(68) Chen, P.-C., and Kuyucak, S. (2012) Developing a comparative docking protocol for the prediction of peptide selectivity profiles: Investigation of potassium channel toxins. *Toxins 4*, 110−138.
(69) Visan, V., Fajloun, Z., Sabatier, J. M., and Grissmer, S. (2004) Mapping of maurotoxin binding sites on hKv1.2, hKv1.3, and hIKCa1 channels. *Mol. Pharmacol. 66*, 1103−1112.
(70) Savarin, P., Romi-Lebrun, R., Zinn-Justin, S., Lebrun, B., Nakajima, T., Gilquin, B., and Menez, A. (1999) Structural and functional consequences of the presence of a fourth disulfide bridge in the scorpion short toxins: Solution structure of the potassium channel inhibitor HsTX1. *Protein Sci. 8*, 2672−2685.